Mon. Not. R. Astron. Soc. **000**, 1–12 (2009) Printed 11 February 2010 (MN LATEX style file v2.2)

Analytical approximations of K-corrections in optical and near-infrared bands

Igor V. Chilingarian[1,2,3⋆], Anne-Laure Melchior[1,4] and Ivan Yu. Zolotukhin[2]
[1] *Observatoire de Paris, LERMA, CNRS UMR 8112, 61 Av. de l'Observatoire, 75014 Paris, France*
[2] *Sternberg Astronomical Institute, Moscow State University, 13 Universitetskij prospect, 119992, Moscow, Russia*
[3] *Centre de données astronomiques de Strasbourg, Observatoire astronomique de Strasbourg, UMR 7550, Université de Strasbourg / CNRS, 11 rue de l'Université, 67000 Strasbourg, France*
[4] *Université Pierre et Marie Curie - Paris 6, 4 Place Jussieu, 75252 Paris Cedex 5, France*

Accepted 2010 February 10. Received 2010 February 01; in original form 2009 August 14

ABSTRACT
To compare photometric properties of galaxies at different redshifts, the fluxes need to be corrected for the changes of effective rest-frame wavelengths of filter bandpasses, called K-corrections. Usual approaches to compute them are based on the template fitting of observed spectral energy distributions (SED) and, thus, require multi-colour photometry. Here, we demonstrate that, in cases of widely used optical and near-infrared filters, K-corrections can be precisely approximated as two-dimensional low-order polynomials of *only* two parameters: *redshift and one observed colour*. With this minimalist approach, we present the polynomial fitting functions for K-corrections in SDSS *ugriz*, UKIRT WFCAM $YJHK$, Johnson-Cousins $UBVR_cI_c$, and 2MASS JHK_s bands for galaxies at redshifts $Z < 0.5$ based on empirically-computed values obtained by fitting combined optical-NIR SEDs of a set of 10^5 galaxies constructed from SDSS DR7 and UKIDSS DR5 photometry using the Virtual Observatory. For luminous red galaxies we provide K-corrections as functions of their redshifts only. In two filters, g and r, we validate our solutions by computing K-corrections directly from SDSS DR7 spectra. We also present a K-corrections calculator, a web-based service for computing K-corrections on-line.

Key words: galaxies: (classification, colours, luminosities, masses, radii, etc.) – galaxies: photometry – galaxies: evolution – galaxies: stellar content – galaxies: fundamental parameters

1 INTRODUCTION

Extragalactic studies usually require comparison between photometric data for different galaxy samples, in particular, comparing measurements obtained for distant galaxies to the local Universe, where properties of galaxies are studied in a much greater detail. Generally, any differences in observable parameters arise from: (1) astrophysical properties of galaxies and (2) observational biases. The former ones include the galaxy evolution effects: due to the light travel time, we see distant galaxies as they were looking several Gyr ago, so the evolution during the last period of their lifetime simply cannot be observed. On the other hand, observational biases arise from the process how the observations are carried out and, therefore, change drastically from one facility to another, even assuming the data are perfectly reduced and calibrated. These include effects of aperture, spatial resolution, and a family of effects connected to the photometric bandpasses.

Photometric data often originate from different observational studies exploiting different photometric systems and, thus require colour transformations to be applied (e.g. Fukugita et al. 1995). But even if the data are obtained in the course of one given project, a galaxy sample may contain objects at different redshifts.

In a broad wavelength range, from ultra-violet to near-infrared, the spectral energy distributions (SED) of non-active galaxies are mostly determined by their stellar population properties, i.e. age and chemical composition, and effects of internal dust attenuation increasing dramatically at short wavelengths (Calzetti et al. 1994; Fitzpatrick 1999). Stellar population SEDs are very far from flat distributions and exhibit prominent features (e.g. Fioc & Rocca-Volmerange 1997; Bruzual & Charlot 2003). At the same time, redshifting the galaxy spectrum is equivalent to shifting the corresponding filter transmission curve. This ex-

⋆ E-mail: Igor.Chilingarian@astro.unistra.fr; chil@sai.msu.ru

plains the difference in fluxes in the same bandpass for two hypothetical galaxies having exactly identical SEDs but being at different redshifts. Historically, this difference is called K-correction (Oke & Sandage 1968). The K-correction formalism is presented in detail and thoroughly discussed in Hogg et al. (2002); Blanton & Roweis (2007).

Nowadays, in the era of large wide-area photometric and spectroscopic extragalactic surveys, the precise, fast and simple computation of K-corrections has become a crucial point for the successful astrophysical interpretation of data. Several approaches were presented in the literature (Fukugita et al. 1995; Mannucci et al. 2001; Blanton & Roweis 2007; Roche et al. 2009). Blanton & Roweis (2007) provide a software package to compute K-corrections for datasets in any photometric system. However, since their method is based on the SED fitting technique, the results critically depend on the availability of multi-colour photometric data. Fukugita et al. (1995) and Mannucci et al. (2001) provide only qualitative dependence of K-corrections on redshift and galaxy morphological type; the latter is very difficult to assess in an automatic way and these methods therefore require availability of original galaxy images in addition to photometric measurements.

The aim of our study is to explore the parameter space of typical observed galaxy properties and to provide simple and precise analytical approximations of K-corrections in widely used optical and NIR photometric bandpasses, based on the minimal set of observables. To achieve this goal, we exploit a large homogeneous database of optical-to-NIR galaxy SEDs compiled from modern wide-area photometric surveys. In the next section, we describe our galaxy sample, details on the computation of K-corrections using PEGASE.2 stellar population models (Fioc & Rocca-Volmerange 1997) and comparison of obtained values with those computed using the KCORRECT code (Blanton & Roweis 2007). In Section 3, we describe analytical approximations, and the validation of our results using spectral-based K-corrections. In Section 4, we compare our results with the literature and briefly discuss some astrophysical interpretation of our technique. Appendices provide tables with coefficients of best-fitting polynomials and present a "K-corrections calculator" service.

2 EMPIRICAL COMPUTATION OF K-CORRECTIONS

2.1 Galaxy sample

We compute K-corrections using a large sample of optical-to-NIR SEDs of nearby galaxies constructed using Virtual Observatory technologies to retrieve and combine photometric measurements from Sloan Digital Sky Survey Data Release 7 (SDSS DR7, Abazajian et al. 2009) and the UKIRT Infrared Deep Survey Data Release 5 (UKIDSS DR5, Lawrence et al. 2007). Comprehensive description of this multi-colour photometric catalogue will be provided in a separate paper (Chilingarian et al. in prep), here we give a brief summary essential for understanding the empirical K-correction computations.

We constructed a sample of galaxies excluding broad-line active galactic nuclei (AGN) by performing the spatial cross-matching of the SDSS DR7 spectroscopic sample in stripes 9 to 16 with the Large Area Survey catalogue of UKIDSS DR5. We selected 190,275 galaxies having spectroscopic redshifts in a range $0.03 < Z < 0.6$ provided by SDSS DR7 using the SDSS CASJobs Service[1]. The spatial cross-identification with UKIDSS DR5 with a search radius of 3 arcsec selecting the best positional matches in case of multiple objects within this radii resulted in 170,533 objects, 87,161 of which were detected in all four UKIDSS Large Area Survey photometric bands (Y, J, H, and K).

In order to compute K-corrections, the photometric measurements from the two data sources have to be homogeneous. We use SDSS fibre magnitudes corresponding to $d = 3$ arcsec circular apertures (*fiberMags*), and computed the corresponding 3 arcsec aperture magnitudes for UKIDSS objects by linearly interpolating between the values provided for three apertures (2.0, 2.8, and 5.7 arcsec) applying zero-point corrections (Hewett et al. 2006) for converting UKIDSS magnitudes from the Vega into the AB system.

The lower redshift limit, $Z = 0.03$, is selected in order to minimise the aperture effects: at a distance of 120 Mpc, corresponding to this redshift, the 3 arcsec aperture encloses about 1.75 kpc, i.e. significant part of the bulge even for giant galaxies, thus stellar populations in galactic nuclei would not dominate the light. Beyond the selected upper redshift limit, $Z = 0.6$, the fraction of normal galaxies in SDSS significantly decreases, because of the magnitude-limited selection of SDSS spectroscopic targets, and at the same time the quality of absorption-line spectra becomes quite poor.

We use magnitudes in 3 arcsec apertures and not the Petrosian magnitudes to be able to compare them directly with the SDSS DR7 spectra obtained within the same apertures. The median 3 arcsec aperture magnitude uncertainties are 0.01 mag and better for g, r, i, Y, J, H, and K, 0.017 mag for z, and 0.07 mag for the u band respectively. All magnitudes are corrected for the foreground Galactic extinction according to Schlegel et al. (1998).

There are important systematic offsets of unknown origin between SDSS DR7 fibre magnitudes and UKIDSS DR5 photometry in 3 arcsec apertures. We fit 3rd order polynomial using 5 colours starting from $r - i$ and redder except $z - Y$ and compute the offset between the expected $z - Y$ value from the best-fitting polynomial and the observed one. The offset has a mean value of 0.22 mag and a standard deviation of 0.13 mag independent from other parameters (e.g. observed colours and a redshift). We therefore subtract it from all UKIDSS magnitudes. This effect is illustrated in Fig. 1. In the top panel, we display the combined SDSS-UKIDSS SED of some galaxy and its best-matching PEGASE.2 template obtained by the K-correction determination procedure described below. The middle and bottom panels show the residuals between the observed SED and its model, and colours in consequent spectral bands with the best-fitting 3rd order polynomial. From the middle panel, it is clear that the NIR part of the SED is offset by a constant value from the optical part, which is evident as the measured $z - Y$ colour strongly deviates from the fitting polynomial.

[1] http://cas.sdss.org/CasJobs

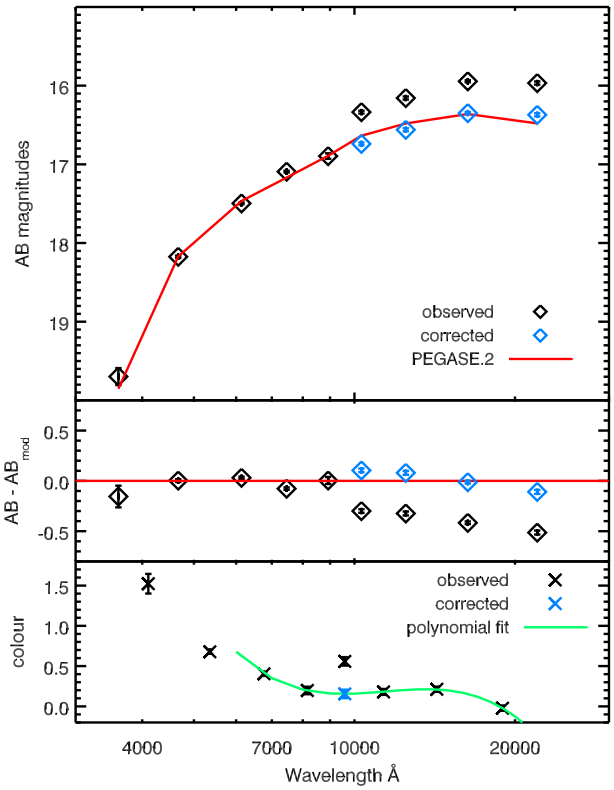

Figure 1. Top panel presents the optical-to-NIR SED of SDSS J155023.03-000023.8 in a 3-arcsec aperture as provided in the catalogue (black diamonds), its NIR part empirically corrected (blue diamonds), its best-matching PEGASE.2 template used for K-correction computation (solid red line). Fitting residuals are shown in middle panel (same symbols). Bottom panel displays colours as a function of wavelength (black crosses), the best-fitting 3rd order polynomial for 5 colours ($r-i$, $i-z$, $Y-J$, $J-H$, and $H-K$) is shown as a solid green line; the corrected value of $z-Y$ is denoted by the blue cross.

2.2 Computation of K-corrections

We used two approaches to compute K-corrections: (1) the KCORRECT software package by Blanton & Roweis (2007) and (2) PEGASE.2-based computations described hereafter. The latter technique allows us to roughly estimate mean stellar population properties as well as internal extinction in galaxies. The analytical fitting is performed for both methods independently.

We first ran the KCORRECT software package to compute the K-corrections for our sample of galaxies. This package is based on a mathematical algorithm, namely non-negative matrix factorisation, which creates model-based template sets. The initial set of hundreds of templates is reduced to a basis of five, which in principle can be used to interpret the galaxy SED in terms of stellar populations. The linear combination of these templates is then fitted into the set of broadband fluxes available for each galaxy to derive the K-corrections in all bands.

Second, we computed a grid of Simple Stellar Populations (SSP) using the PEGASE.2 evolutionary synthesis code (Fioc & Rocca-Volmerange 1997) for a set of 75 ages nearly logarithmically spaced between 25 Myr and 16.5 Gyr and 10

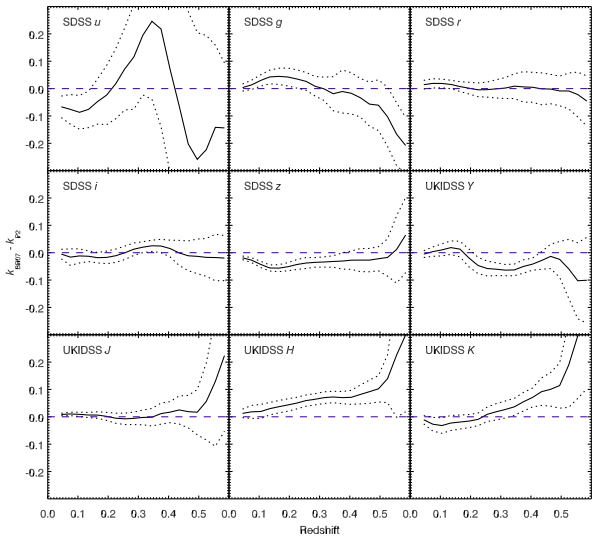

Figure 2. Comparison of empirically calculated K-corrections obtained by fitting the photometric data using PEGASE.2 SSP models (k_{P2}) and by the KCORRECT (k_{BR07}) code. Each panel displays the difference between the two approaches as a function of redshift. Solid lines denote the median differences and their standard deviations are shown with dotted lines.

metallicities between $-2.5 < [\mathrm{Fe/H}] < +1.0$ dex. Such a grid was computed separately for redshifts between $0 < Z < 0.6$ with a step of 0.05. We apply the Fitzpatrick (1999) extinction law for each of 750 SSPs at each redshift varying the A_V between 0 and 2.25 mag with a step of 0.15 mag ending up with 11250 template SEDs per redshift.

In order to compute K-corrections for a given galaxy, we perform a linear interpolation of the SSP grid to its redshift, then pick up the best-matching template SED in terms of χ^2 normalising both data and templates by the mean fluxes in all filters. Since our photometric uncertainties are quite small, this approach would not result in significant biases. Once the best-matching template has been found, the K-corrections in all photometric bands are computed as $K_f(Z) = -2.5\log(F(0)/F(Z))$, where $F(Z)$ and $F(0)$ are fluxes in a given filter at redshift Z and in the restframe. We provide an example of an observed SED and its best-matching template in the upper panel of Fig 1.

Since we can calculate model fluxes in any photometric band, we also used the same technique to compute K-corrections in Johnson-Cousins $UBVR_cI_c$ and 2MASS JHK_s bands.

We compare the values computed in this fashion with the value derived by the KCORRECT code from the same photometric dataset. The comparison for all 9 SDSS-UKIDSS bands is provided in Fig 2.

In general, the results obtained by using the two approaches in $ugrizYJHK$ bands are quite similar. However, in certain spectral bands, some statistically significant differences are evident. The worst situation is observed in the SDSS u band mainly for two reasons: relatively poor quality of the u band photometry especially for objects at higher redshifts and very high sensitivity of UV colours to even low mass fractions of recently formed stars, which affect fluxes at longer wavelengths much weaker. Therefore, the SSP fitting

approach presumably should not work well. At the same time, the linear combination of 5 templates used by the KCORRECT package may also produce significant biases due to age and/or metallicity mismatch between the templates and real galaxies. Finally, we provide the K-corrections for the u band, emphasising that since no independent verification is possible in our case, one has to use these results with caution. The same statement applies to K band K-corrections, although the results of the two approaches well match each other, because the computation relies on the extrapolation of galaxy SED in the NIR part, where stellar population models and, correspondingly, the template spectra are of much lower quality than in the optical wavelength domain.

Computations in the r, i, and J bands agree remarkably well except the high-redshift ($Z > 0.5$) end of the J band. There are some systematic discrepancies between the two techniques in the g, z, Y, and H bands. They may originate from the fact that PEGASE.2 SSPs are built using the theoretical stellar library, shown to introduce colour differences between synthetic spectra and observed ones at least in the SDSS photometric system (Maraston et al. 2009). We will analyse the g and r band results below using direct spectral-based K-corrections, while for the remaining bandpasses no independent test can be performed since no large samples of galaxy spectra are available in those wavelength domains. However, we note that the discrepancies are an order of 0.05 mag, hence, both approaches may be used in the photometric studies. Therefore, we will proceed with the rest of our analysis using both techniques of the K-correction computation, addressing them as *BR07* and *SSP* for the KCORRECT and PEGASE.2 SSP-based approaches respectively.

3 RESULTS

3.1 Analytical approximations

We observe a large scatter of K-corrections as functions of redshift reaching 2 mag in all SDSS-UKIDSS bands except H and K. However, exploring the data with the TOPCAT software[2], we found that adding just one observed colour as a second parameter and approximating the K-correction as a surface in the three-dimensional space, significantly reduces the residual scatter bringing it to the order of K-correction computation uncertainties. We fit K-correction values in every filter q as a polynomial surface of a form:

$$K_q(Z, m_{f_1} - m_{f_2}) = \sum_{x=0}^{N_Z} \sum_{y=0}^{N_c} a_{x,y} Z^x (m_{f_1} - m_{f_2})^y, \qquad (1)$$

where $a_{x,y}$ are polynomial coefficients, Z is a spectroscopic redshift, m_{f_1} and m_{f_2} are observed magnitudes in filters f_1 and f_2 chosen for every filter q, N_Z and N_c are empirically selected polynomial powers in the redshift and colour dimensions respectively. Given that K-corrections are zero by definition at $Z = 0$, no constant term is needed and all $a_{0,y} = 0$.

[2] http://www.star.bris.ac.uk/∼mbt/topcat/

Since both K-correction computation techniques used in our study are based on the stellar population models, and our analytical approximations exploit simple polynomial fitting technique without any clipping of outliers, we have to exclude strong active galactic nuclei (AGN) and quasars, as well as SDSS targeting artifacts (e.g. aircrafts, satellites, minor planets) and objects with wrong redshift determinations, which may affect our best-fitting solutions. We have fitted all 190,275 SDSS DR7 spectra using the NBURSTS full spectral fitting technique (Chilingarian et al. 2007b,a) in the restframe wavelength range between 3900 and 6750Å, and selected for our further analysis only 164,108 objects having reduced $\chi^2/DOF < 0.9$ (median $\chi^2/DOF = 0.67$, which is smaller than unity because of slight spectral oversampling of SDSS data). The interpretation of the spectral fitting results will be provided together with the presentation of a spectrophotometric catalogue in Chilingarian et al. (in prep).

We computed and fitted K-corrections in this fashion for a sample of 164,108 SDSS DR7 galaxies with well-fitted spectra using only SDSS 5-bands photometry, and to the merged SDSS–UKIDSS sample containing photometric information in all 9 bands for 74,254 galaxies. While the results from the two approaches remain nearly statistically identical in u, g, and r bands, the difference becomes significant in i and especially in z. Two distinct sequences become clear in the redshift vs K-correction plots in i and z in case of the 5-bands based computation. Only one of the two sequences remains in each case if full 9-band SEDs are used, suggesting that the second sequence is created by wrong stellar population templates picked up from the template grid. This clearly demonstrates the importance of the NIR part to compute K-corrections if using a fully empirical approach. Consequently, r.m.s of the polynomial surface fitting residuals in case of 9-bands based K-corrections in the z band is four times smaller compared to the 5 bands.

In Fig 3–4, we display the analytical approximations of K-corrections in 9 bands for the values computed using PEGASE.2-based matching and the KCORRECT code. Upper panels demonstrate computed values as a function of redshift and an observed colour, colour-coded according to the scale bars presented in the plots. The lower panels display the mean residuals and their r.m.s. as a function of redshift. Since we use a fixed grid of PEGASE.2 templates and do not perform interpolation on the age and metallicity axes, the individual template age sequences become visible at high redshifts range in some filters (e.g. Y). However, the computational errors due to this discretisation do not exceed 0.03 mag. Black lines in the plots denote the behaviour of K-corrections for galaxies having fixed restframe (i.e. K-corrected) $g - r$ colours. Solid lines are for $0.73 < g-r < 0.81$ mag, dashed for $0.58 < g-r < 0.70$ mag, dot-dashed for $0.4 < g - r < 0.6$ mag, and triple-dot-dashed for $g-r < 0.15$ mag, roughly corresponding to luminous red galaxies (LRG), early-type spirals (S-early), late-type spirals (S-late), and actively star-forming galaxies (SF). These lines are constructed by connecting median values within 0.03-wide redshift bins in the colour bins given above. We notice that the u-band K-corrections computed with the KCORRECT code at higher redshifts turn to be higher than expected for LRGs defined by $g-r$ restframe colours, which is probably indicative of a template mismatch.

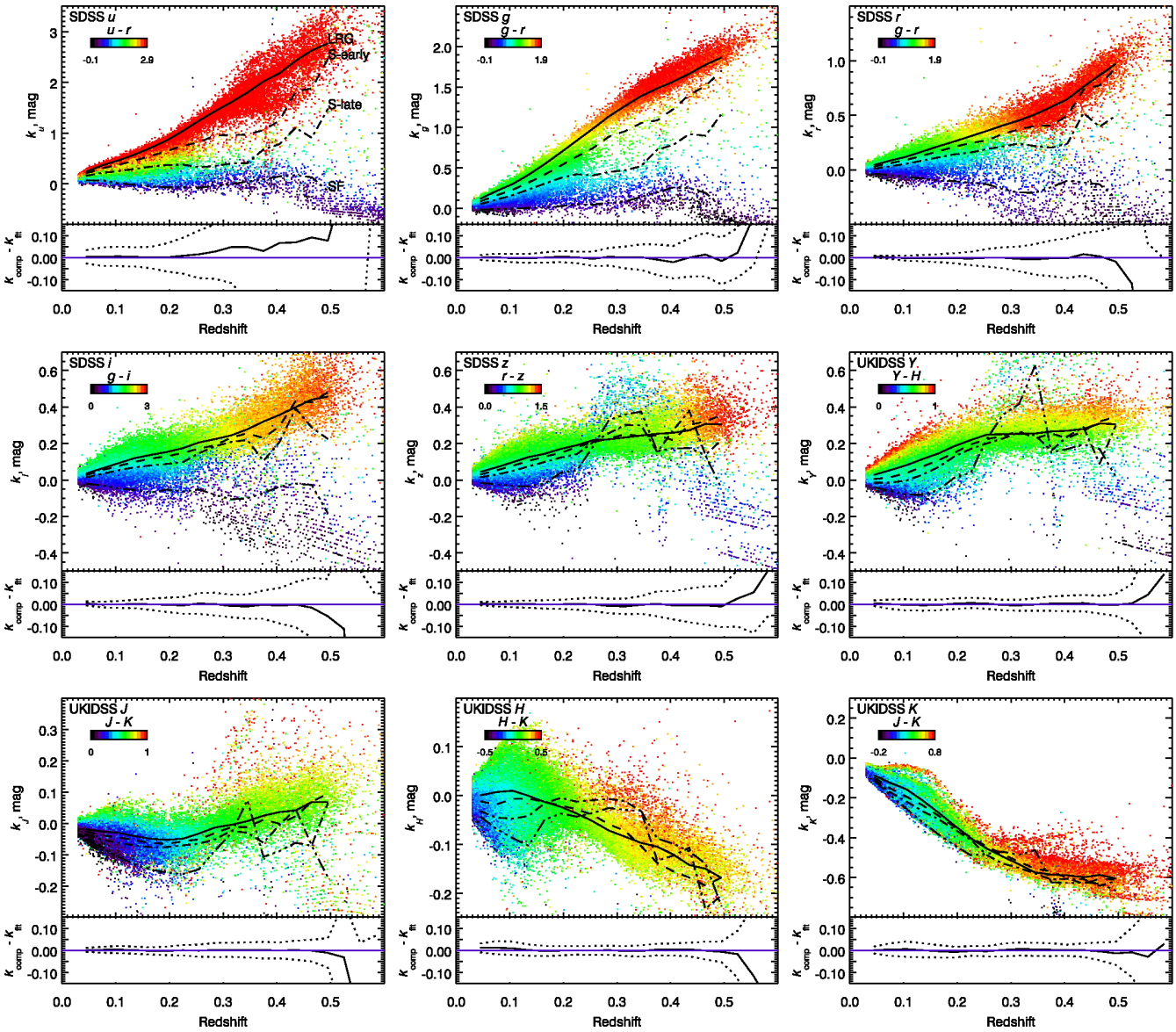

Figure 3. K-corrections in 9 photometric SDSS-UKIDSS bands computed using PEGASE.2 SSP matching and the residuals of the analytical fitting. Upper panel for each filter presents computed K-corrections vs redshift with a colour-coded observed colour used to perform the fitting. Sequences of galaxies with constant restframe $g-r$ colours roughly corresponding to different morphological types are overplotted (see the text for details). Lower panels display the residual between the analytical approximation and measured values (bold black line) and r.m.s. of the fitting residuals (dotted lines).

The 4 morphological types are well separated in the u, g, and r bands; only very blue objects exhibit a distinguished behaviour in i, while in NIR bands the K-corrections become nearly independent of a restframe colour of a galaxy (or its morphological type).

Some tables containing the coefficients of polynomial approximations are provided in Appendix A. Additional tables for K-correction approximations using different observed colours are provided on the "K-corrections calculator" web-site described in Appendix B.

Classical Johnson-Cousins photometric system is still widely used for extragalactic research, as well as NIR bands of the 2MASS survey (Skrutskie et al. 2006), therefore computation and analytical approximation of K-corrections in these bands are of a great practical importance. However, we do not have photometric measurements for galaxies in our sample obtained in these bands. We used the photometric transformations defined in Jordi et al. (2006) for stars and those provided on the web-pages of SDSS in order to convert available SDSS *ugriz* magnitudes into Johnson-Cousins $UBVR_cI_c$, and UKIDSS $YJHK$ to 2MASS JHK_s transformations presented in Hewett et al. (2006). Then, we used these magnitudes to fit K-corrections in the $UBVR_cI_c$ and 2MASS JHK_s bands as functions of "computed" observed colours defined in the same photometric system. The coefficients of these polynomial approximations are available at the "K-corrections calculator" web-site. We note that the approximations for the Johnson–Cousins and 2MASS filters

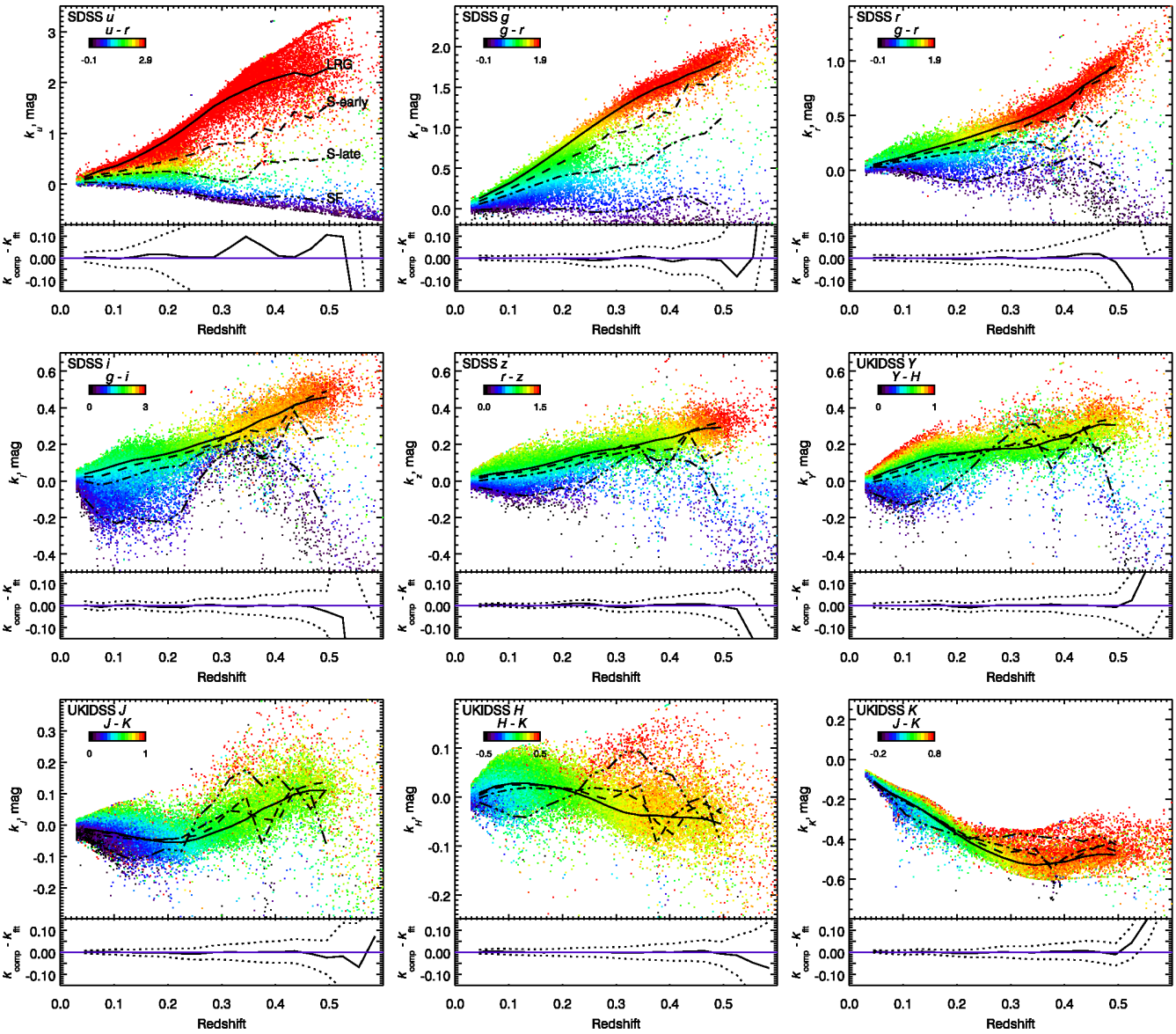

Figure 4. The same as Fig 3, but the K-corrections are computed using the KCORRECT code.

are provided as functions of colours in the Vega system, whereas for SDSS and UKIRT WFCAM bands the colours are expressed in AB magnitudes.

3.2 Validation using SDSS DR7 spectra

We fetched optical SDSS spectra in the wavelength range between 3800 and 9200Å for all galaxies from our sample, therefore we were able to perform independent direct verification of the analytical approximations of K-corrections presented above. The available spectral coverage allows us to compute fluxes directly from the spectra using both real and redshifted filter transmission curves, i.e. to obtain real restframe fluxes, for g, r, and i filters. The highest redshifts, where reliable computation is still possible for the r and i bands are ~ 0.28 and ~ 0.08 respectively due to the upper wavelength limit of the SDSS spectral coverage. We use a similar technique to Roche et al. (2009) for the computation of spectral-based K-corrections, with two main differences: (1) we redshift the filter transmission curves instead of blueshifting the spectra in order to prevent interpolation of fluxes and smoothing defects in the spectra; (2) in case of missing data within the wavelength range, we interpolate fluxes linearly or extrapolate them using constant level in F_λ if the red tail of the redshifted filter transmission curve goes beyond 9200Å. The maximal adopted truncation of the filter transmission curve was at a level of 1 per cent of the maximal transmission.

In Fig 5, we present the differences between spectral-based K-corrections in g and r bands and the analytical approximations of those computed empirically from SDSS *fiberMag* using PEGASE.2 SSP templates and the KCORRECT code as functions of redshift and observed $g-r$ colour. In the r band, the agreement between spectral-based K-corrections and analytical fitting derived above is as good as 0.02 mag. For the low-redshift ($Z < 0.3$) part of the sample, the situ-

ation is similar in the g band, although the systematic difference reaches 0.06 mag. However, for the higher redshifts ($0.3 < Z < 0.5$), the discrepancies become as large as 0.15–0.2 mag. This inconsistency possibly originates from underestimated g synthetic magnitudes due to a very low signal in the blue part of the spectra for objects having $Z > 0.3$. Formally computed photometric errors of synthetic g magnitudes in this redshift range reach 0.2 mag.

4 DISCUSSION AND CONCLUSIONS

4.1 Comparison with literature

We compare K-corrections computed in this study with the results described in literature. Fukugita et al. (1995) presented K-corrections of the SDSS photometric system in their fig. 20. Since no data are provided in the numerical form, we are able to compare the results only qualitatively. The behaviour of the values as functions of redshifts agree well at $Z < 0.5$, different morphological types of galaxies in Fukugita et al. (1995) are related to the reconstructed restframe colours. The elliptical galaxy template of Fukugita et al. (1995) behaves similarly to the sequences denoted as "LRG" in Fig. 3–4 corresponding to luminous red galaxies. We notice that the filter transmission curves used in Fukugita et al. (1995) are somewhat different from those obtained from the telescope and presented at the SDSS DR7 web pages, especially for the g and r bands, explaining why the exact match between the two approaches cannot be achieved.

Mannucci et al. (2001) present in their fig. 7 NIR K-corrections computed from the templates spectra of galaxies having different morphological types computed with the PEGASE code. Although their JHK bands are slightly different from those of the UKIDSS, the behaviour of K-corrections as functions of redshift is very similar. Authors mention that K-corrections in H and K are virtually insensitive to the galaxy morphological types, which we observe as their very weak dependence on galaxy colours.

We compare our results with the spectral-based K-corrections presented in Roche et al. (2009). The authors deal only with red sequence galaxies, therefore we are able to test only a small although very important part of the parameter space. The values of K-corrections provided in tables 1–2 of Roche et al. (2009) are overplotted in Fig 5. The agreement is remarkably good, which is, however, expected because our spectral-based K-corrections computed in the same manner agree well with the best-fitting solutions.

4.2 Recovered restframe magnitudes and LRGs

It is well known that the restframe colours correlate with the galaxy morphology, and there is a pronounced bimodality in the colour distribution of galaxies (see e.g. Strateva et al. 2001; Baldry et al. 2004; Balogh et al. 2004). The so-called "red sequence" includes elliptical and lenticular galaxies with some fraction of early-type spirals demonstrating a lack of ongoing star formation, whereas the "blue cloud" contains actively star-forming objects represented mostly by late-type spiral and irregular galaxies. Some morphologically

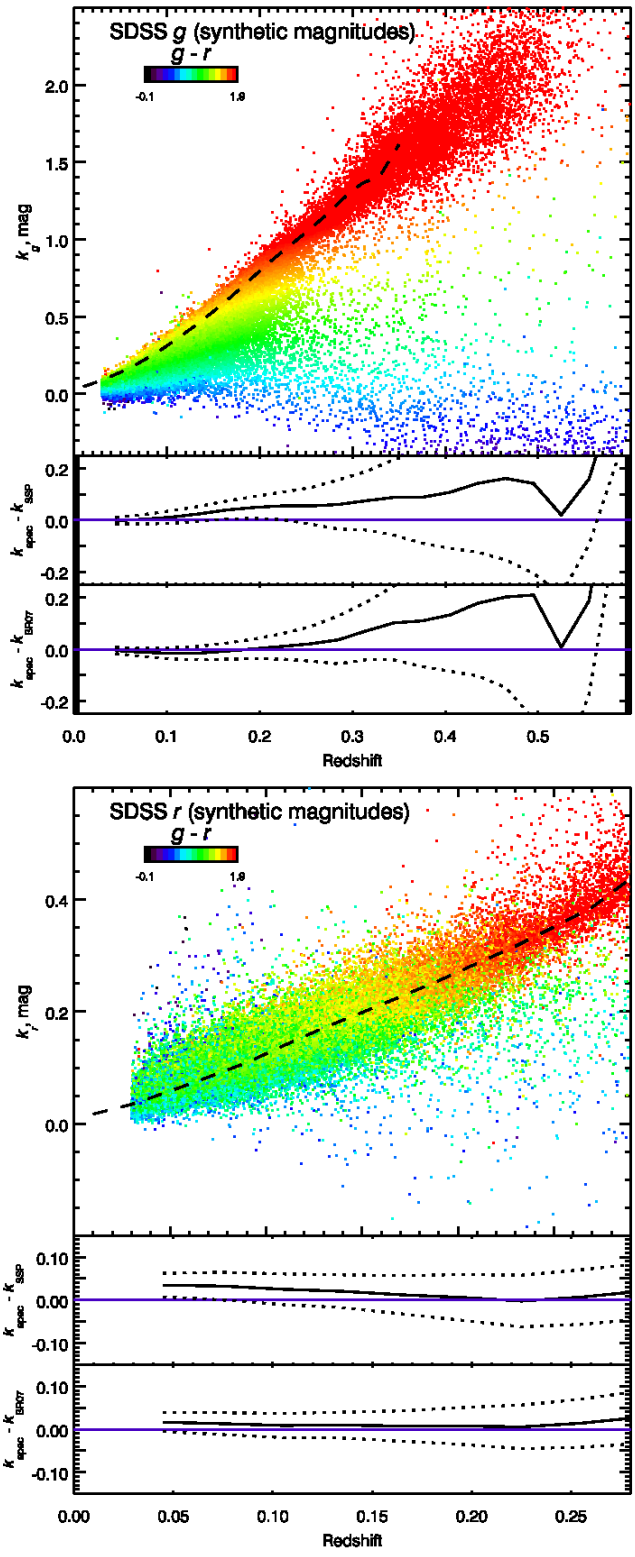

Figure 5. Differences between analytically approximated and directly measured spectral-based K-corrections in the g (top) and r (bottom) bands. Upper panels display computed values of K-corrections. Dashed lines denote spectral-based K-corrections for early-type galaxies presented in Roche et al. (2009). Two bottom panels for each spectral band display the differences between spectral-based K-corrections and those computed using PEGASE.2 SSP matching and the KCORRECT code, respectively.

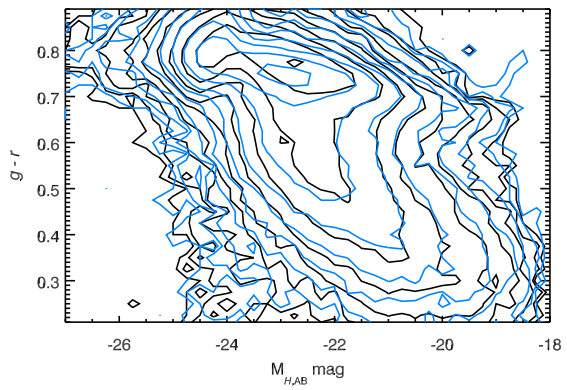

Figure 6. Colour-magnitude diagram presenting data for 74,254 galaxies using the SDSS DR7 and UKIDSS DR5 Petrosian magnitudes in the g, r, and H bands respectively K-corrected using the analytical approximations presented in this study. Black and blue contours are for the PEGASE.2-based and KCORRECT derived values respectively. Levels of the two-dimensional density plot correspond to the powers of two from 2 (outermost) to 1024 (innermost) galaxies per bin of 0.25 mag×0.025 mag.

classified early-type galaxies indeed sit below the red sequence in the "green valley" or even "blue cloud" regions. In Fig 6, we provide the colour-magnitude plot of 74,254 galaxies from SDSS DR7 and UKIDSS, where their total Petrosian magnitudes were K-corrected using the presented analytical approximations.

Some of the objects residing below the red sequence referred as E+A galaxies (Dressler & Gunn 1983; Couch & Sharples 1987; Dressler et al. 1999) often exhibit weak if any emission lines in their spectra ruling out major star formation. However, Balmer absorptions are remarkably deep, which is a good evidence for the presence of young stars that was confirmed by the recent study where authors used full-spectral fitting (Chilingarian et al. 2009b). Despite the early-type morphologies of E+A, these galaxies are indistinguishable from spirals if one uses only integrated colours and therefore, colour transformations and K-corrections behave very similarly for these two morphologically different classes of galaxies. Hence, the restframe colours are not tightly connected to the galaxy morphology, but to the internal properties such as ongoing star formation and, therefore, they are specific of stellar populations. Another example would be dwarf elliiptical (dE) and compact elliptical (cE) galaxies. The former ones usually have intermediate-age stellar populations with metallicities lower than those of LRGs (see e.g. Chilingarian et al. 2008; Chilingarian 2009), therefore their global optical colours are bluer, and their K-corrections in the corresponding bands are lower than those of more massive early-type galaxies, which results in quite a strong tilt of the red sequence at $M_{H,AB} > -20$ mag (see Fig 6) reproducing its behaviour for nearby dE galaxies (Janz & Lisker 2009). On the other hand, cE galaxies with luminosities similar to dEs, originate from the tidal stripping of more massive early-type progenitors and, therefore, exhibit old metal-rich stellar populations (Chilingarian et al. 2009a). For this reason, cEs have significantly redder colours compared to dEs and, therefore, have behaviour of K-corrections very similar to LRGs.

Table 1. Coefficients of the best-fitting polynomials for the redshift-dependence of K-corrections for luminous red galaxies. Initial K-correction values were computed from the PEGASE.2 SSPs.

	Z^1	Z^2	Z^3	Z^4	Z^5
K_u	5.93938	-30.5247	179.473	-380.488	282.011
K_g	2.61617	-4.44391	93.0132	-284.582	252.245
K_r	0.312233	14.3325	-68.2493	136.254	-87.3360
K_i	0.234538	14.3162	-97.2754	246.775	-207.028
K_z	0.897075	3.60112	-34.7890	93.0266	-79.5246
K_Y	0.402992	5.30858	-18.3172	17.6760	-0.31400
K_J	-0.076704	-4.48411	27.1585	-45.6481	22.6928
K_H	0.382926	-1.81590	-13.1657	57.5486	-59.0677
K_K	-1.75997	5.48023	-56.4175	175.939	-160.754

Table 2. Same as in Table 1 but the KCORRECT computed K-corrections.

	Z^1	Z^2	Z^3	Z^4	Z^5
K_u	4.20000	-24.5015	229.149	-574.272	434.901
K_g	2.17470	10.3810	1.49141	-76.6656	88.6641
K_r	0.710579	10.1949	-57.0378	133.141	-99.9271
K_i	0.702681	4.27115	-37.2060	112.054	-105.976
K_z	0.643953	-1.88400	13.6952	-35.0960	29.9249
K_Y	-0.245996	21.8772	-137.019	322.051	-257.136
K_J	0.106358	-5.06024	18.4707	-3.73196	-23.9595
K_H	0.268479	3.03488	-35.8994	98.6524	-83.9401
K_K	-2.80894	15.6923	-96.8401	256.235	-220.691

There is a weak dependence of the colour of red sequence galaxies on the galaxy luminosity reflecting, in particular, a mass-metallicity relation of early-type galaxies. Massive (and luminous) red sequence galaxies compared to lower-mass systems contain more metal-rich stellar populations having intrinsically redder colours than the metal-poor ones.

The special case of LRGs is very important for understanding galaxy formation and evolution, therefore we provide specific approximations for these objects. Since the intrinsic spread of LRGs restframe colours is very low, about 0.04 mag, their K-corrections can be well approximated as a function of a single parameter, the redshift. We selected a sample of LRGs based on their restframe colours, and fitted the K-corrections as polynomial functions of their redshifts in all 9 photometric bands. The coefficients of best-fitting 5th order polynomials with no constant term are presented in Table 1 and Table 2 for the PEGASE.2 SSP-based and KCORRECT-computed values correspondingly. Every row corresponds to a given photometric band and contains coefficients from the 1st to the 5th power of redshift.

Rest-frame colours of LRGs provide a natural test for the quality of K-corrections. The vast majority of stars in these objects is believed to form on short timescales in the early Universe and then evolve passively. The redshift $z = 0.5$ corresponds to the lookback time about 5 Gyr. Thus, if one assumes LRGs to be as old as 12 Gyr in the local Universe and contain no younger stars, then at $z = 0.5$ their restframe optical colours would be slightly bluer with the differences $\Delta(u-r) \approx 0.25$ mag, $\Delta(g-r) \approx 0.08$ mag, and redder colours different by less than 0.03 mag (values estimated from the colour evolution of the solar metallicity

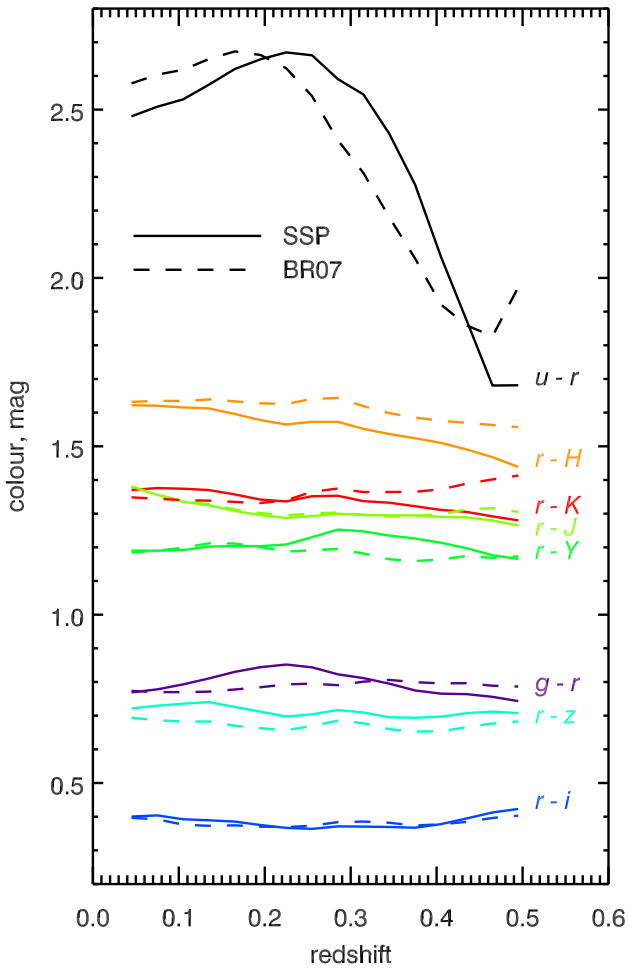

Figure 7. Dependence of recovered restframe colours of LRGs on redshift. Solid and dashed lines are for the PEGASE.2 SSP-based and KCORRECT computed K-corrections respectively.

PEGASE.2 SSP). In Fig 7, we present the behaviour of recovered restframe colours of LRGs as functions of redshift. All presented colours have SDSS r as one of the bands, because the best consistency of both K-correction computation algorithms is reached in this band.

The bluest $u-r$ colour exhibits significant changes over redshift exceeding by a factor of 3 the expectations from the passive evolution of a SSP. This, however, can be explained by a "tail" of the star formation history since even small mass fractions of intermediate mass stars strongly affect the u band photometry. On the other hand, we cannot exclude the template mismatch between the model and real galaxies to be partly responsible for this effect.

Surprisingly, the $g-r$ colour does not evolve at all if we use the KCORRECT values of g-band K-corrections, but evolves slightly stronger than expected from the SSP evolution when using the PEGASE.2 based values, being somewhat consistent with the $u-r$ colour behaviour.

While $r-i$ and $r-z$ colours behave similarly in both approaches exhibiting, as expected, virtually no evolution, in NIR bands the situation is different. Both techniques are consistent in the J band, although demonstrating rather unexpected evolution by about 0.08 mag, whereas in H and K they are significantly different (as also can be seen from the corresponding panels in Fig. 2). The PEGASE.2 SSP-based K-band K-corrections at $Z > 0.3$ look slightly underestimated, conversely to the KCORRECT-computed ones, which are overestimated. In the H band, both methods seem to underestimate K-corrections, but SSP-based approach is stronger affected.

The decisive answer to the questions about the K-correction computation in NIR bands will be given only when the next generation NIR stellar population models based on empirical stellar libraries become available. The H and K band solutions presented in this paper have to be used with caution keeping in mind that some systematic errors may be introduced to the final results.

4.3 Summary

We present polynomial approximations of K-corrections in commonly used optical (SDSS *ugriz* and Johnson-Cousins $UBVR_cI_c$) and near-infrared (UKIRT WFCAM $YJHK$ and 2MASS JHK_s) broad-band filters as functions of redshift and observed colours for galaxies at redshifts $Z < 0.5$. The traditional K-correction computation techniques based on the SED fitting require multi-colour photometry, which is not always available. Our approach allows one to compute restframe galaxy magnitudes of the same quality using a minimal set of observables including only two photometric points and a redshift. For luminous red galaxies, we provide the fitting solutions of K-corrections as 1-dimensional polynomial functions of a redshift.

ACKNOWLEDGMENTS

In this study, we used the UKIDSS DR5 survey catalogues available through the WFCAM science archive and SDSS DR7 data. Funding for the SDSS and SDSS-II has been provided by the Alfred P. Sloan Foundation, the Participating Institutions, the National Science Foundation, the U.S. Department of Energy, the National Aeronautics and Space Administration, the Japanese Monbukagakusho, the Max Planck Society, and the Higher Education Funding Council for England. The SDSS Web Site is http://www.sdss.org/. We acknowledge the usage of the TOPCAT software by M.Taylor. IC and IZ acknowledge the support from the RFBR grants 07-02-0029 and 09-02-00032. Special thanks to A. Sergeev for the "K-corrections calculator" web-site design. This research is supported by the VO Paris Data Centre. We thank our anonymous referee for useful suggestions.

REFERENCES

Abazajian, K. N., et al. 2009, ApJS, 182, 543
Baldry, I. K., Glazebrook, K., Brinkmann, J., Ivezić, Ž., Lupton, R. H., Nichol, R. C., & Szalay, A. S. 2004, ApJ, 600, 681
Balogh, M. L., Baldry, I. K., Nichol, R., Miller, C., Bower, R., & Glazebrook, K. 2004, ApJ, 615, L101
Blanton, M. R. & Roweis, S. 2007, AJ, 133, 734
Bruzual, G. & Charlot, S. 2003, MNRAS, 344, 1000

Calzetti, D., Kinney, A. L., & Storchi-Bergmann, T. 1994, ApJ, 429, 582
Chilingarian, I., Cayatte, V., Revaz, Y., Dodonov, S., Durand, D., Durret, F., Micol, A., & Slezak, E. 2009a, Science, 326, 1379
Chilingarian, I., Prugniel, P., Sil'chenko, O., & Koleva, M. 2007a, in IAU Symposium, Vol. 241, Stellar Populations as Building Blocks of Galaxies, ed. A. Vazdekis & R. R. Peletier (Cambridge, UK: Cambridge University Press), 175–176, arXiv:0709.3047
Chilingarian, I. V. 2009, MNRAS, 394, 1229
Chilingarian, I. V., Cayatte, V., Durret, F., Adami, C., Balkowski, C., Chemin, L., Laganá, T. F., & Prugniel, P. 2008, A&A, 486, 85
Chilingarian, I. V., De Rijcke, S., & Buyle, P. 2009b, ApJ, 697, L111
Chilingarian, I. V., Prugniel, P., Sil'chenko, O. K., & Afanasiev, V. L. 2007b, MNRAS, 376, 1033
Couch, W. J. & Sharples, R. M. 1987, MNRAS, 229, 423
Dressler, A. & Gunn, J. E. 1983, ApJ, 270, 7
Dressler, A., Smail, I., Poggianti, B. M., Butcher, H., Couch, W. J., Ellis, R. S., & Oemler, A. J. 1999, ApJS, 122, 51
Fioc, M. & Rocca-Volmerange, B. 1997, A&A, 326, 950
Fitzpatrick, E. L. 1999, PASP, 111, 63
Fukugita, M., Shimasaku, K., & Ichikawa, T. 1995, PASP, 107, 945
Hewett, P. C., Warren, S. J., Leggett, S. K., & Hodgkin, S. T. 2006, MNRAS, 367, 454
Hogg, D. W., Baldry, I. K., Blanton, M. R., & Eisenstein, D. J. 2002, arXiv:astro-ph/0210394
Janz, J. & Lisker, T. 2009, ApJ, 696, L102
Jordi, K., Grebel, E. K., & Ammon, K. 2006, A&A, 460, 339
Lawrence, A., et al. 2007, MNRAS, 379, 1599
Mannucci, F., Basile, F., Poggianti, B. M., Cimatti, A., Daddi, E., Pozzetti, L., & Vanzi, L. 2001, MNRAS, 326, 745
Maraston, C., Strömbäck, G., Thomas, D., Wake, D. A., & Nichol, R. C. 2009, MNRAS, 394, L107
Oke, J. B. & Sandage, A. 1968, ApJ, 154, 21
Roche, N., Bernardi, M., & Hyde, J. 2009, MNRAS, 398, 1549
Schlegel, D. J., Finkbeiner, D. P., & Davis, M. 1998, ApJ, 500, 525
Skrutskie, M. F., et al. 2006, AJ, 131, 1163
Strateva, I., et al. 2001, AJ, 122, 1861

APPENDIX A: 2-DIMENSIONAL APPROXIMATIONS OF K-CORRECTIONS

Here we provide tables containing coefficients of the analytical approximations of K-corrections. Columns in every table contain colour terms of the fitting solution, from constant to the 3rd order respectively. Rows are for the redshift dependence. The maximal degree of the polynomial surface is set to 5 or 7 (for the H band), therefore the coefficients for the higher degrees, in both colour and redshift, are set to zero. Tables A1–A9 and A10–A18 present the coefficients for approximations of PEGASE.2-based and KCORRECT-computed K-corrections in the SDSS *ugriz* and UKIDSS $YJHK$ bands. Tables A19–A23 contain the coefficients for approximations of PEGASE.2-based K-corrections in the Johnson–Cousins $UBVR_cI_c$ bands. The coefficients for the 2MASS JHK_s bands as well as for the other colour combinations of SDSS and UKIDSS bands are provided online through the "K-corrections calculator" service.

Table A1. The coefficients $a_{x,y}$ of the two-dimensional polynomial approximation of K-corrections $K_u(Z, u-r)$ in the SDSS u band (see Equation 1). In order to derive a value for K_u, one needs to sum the polynomial terms of a form Z^x and $(u-r)^y$ from the table heading and its first column multiplied by the coefficients in corresponding table cells.

	$(u-r)^0$	$(u-r)^1$	$(u-r)^2$	$(u-r)^3$
Z^0	0	0	0	0
Z^1	1.63349	2.24658	0.141845	-0.13441
Z^2	-71.84	20.4939	-3.82771	0.789867
Z^3	257.509	-42.3042	-4.05721	0
Z^4	-308.573	63.0036	0	0
Z^5	42.8572	0	0	0

Table A2. Same as in Table A1 but for the SDSS g band as a function of redshift and the $g-r$ colour.

	$(g-r)^0$	$(g-r)^1$	$(g-r)^2$	$(g-r)^3$
Z^0	0	0	0	0
Z^1	-0.900332	3.97338	0.774394	-1.09389
Z^2	3.65877	-8.04213	11.0321	0.781176
Z^3	-16.7457	-31.1241	-17.5553	0
Z^4	87.3565	71.5801	0	0
Z^5	-123.671	0	0	0

Table A3. Same as in Table A1 but for the SDSS r band as a function of redshift and the $g-r$ colour.

	$(g-r)^0$	$(g-r)^1$	$(g-r)^2$	$(g-r)^3$
Z^0	0	0	0	0
Z^1	-1.61294	3.81378	-3.56114	2.47133
Z^2	9.13285	9.85141	-5.1432	-7.02213
Z^3	-81.8341	-30.3631	38.5052	0
Z^4	250.732	-25.0159	0	0
Z^5	-215.377	0	0	0

Table A4. Same as in Table A1 but for the SDSS i band as a function of redshift and the $g-i$ colour.

	$(g-i)^0$	$(g-i)^1$	$(g-i)^2$	$(g-i)^3$
Z^0	0	0	0	0
Z^1	-2.41799	4.68318	-3.70678	1.5155
Z^2	11.2598	5.14198	-2.64767	-3.63215
Z^3	-94.7387	-14.154	27.2864	0
Z^4	285.775	-51.6662	0	0
Z^5	-222.641	0	0	0

Table A5. Same as in Table A1 but for the SDSS z band as a function of redshift and the $r-z$ colour.

	$(r-z)^0$	$(r-z)^1$	$(r-z)^2$	$(r-z)^3$
Z^0	0	0	0	0
Z^1	-1.7252	3.35566	0.469411	0.350873
Z^2	14.9772	-23.1956	-3.32427	1.78842
Z^3	-41.1269	75.2648	-10.2986	0
Z^4	11.3667	-48.3299	0	0
Z^5	23.5438	0	0	0

Table A6. Same as in Table A1 but for the UKIDSS Y band as a function of redshift and the $Y-H$ colour.

	$(Y-H)^0$	$(Y-H)^1$	$(Y-H)^2$	$(Y-H)^3$
Z^0	0	0	0	0
Z^1	-2.01575	2.70429	6.01384	-5.17119
Z^2	14.3112	-13.2354	-4.03961	13.2633
Z^3	-46.4835	12.7464	-26.3263	0
Z^4	80.2341	27.9842	0	0
Z^5	-66.1958	0	0	0

Table A7. Same as in Table A1 but for the UKIDSS J band as a function of redshift and the $J-K$ colour.

	$(J-K)^0$	$(J-K)^1$	$(J-K)^2$	$(J-K)^3$
Z^0	0	0	0	0
Z^1	-0.765217	2.43055	-0.427304	0.277662
Z^2	1.59864	-14.646	12.0911	-1.2131
Z^3	-4.02136	18.077	-26.1137	0
Z^4	18.5608	25.2691	0	0
Z^5	-40.3567	0	0	0

Table A8. Same as in Table A1 but for the UKIDSS H band as a function of redshift and the $H-K$ colour.

	$(H-K)^0$	$(H-K)^1$	$(H-K)^2$	$(H-K)^3$
Z^0	0	0	0	0
Z^1	-0.642942	-1.05192	-15.5123	-18.1957
Z^2	26.3667	80.0291	192.688	179.956
Z^3	-274.11	-564.952	-848.543	-646.653
Z^4	1081	1569.47	1741.31	761.264
Z^5	-1938.48	-1893.45	-1488.4	0
Z^6	1448.38	869.396	0	0
Z^7	-249.952	0	0	0

Table A9. Same as in Table A1 but for the UKIDSS K band as a function of redshift and the $J-K$ colour.

	$(J-K)^0$	$(J-K)^1$	$(J-K)^2$	$(J-K)^3$
Z^0	0	0	0	0
Z^1	-2.80374	4.14968	1.15579	-1.94003
Z^2	13.4077	-39.5749	11.7	4.7809
Z^3	-69.7725	94.0769	-35.1023	0
Z^4	157.649	-44.0291	0	0
Z^5	-132.317	0	0	0

Table A10. Same as in Table A1 but using the KCORRECT code.

	$(u-r)^0$	$(u-r)^1$	$(u-r)^2$	$(u-r)^3$
Z^0	0	0	0	0
Z^1	8.81624	-12.0027	5.57928	-0.825005
Z^2	33.0392	39.7152	-18.7077	4.0901
Z^3	-1223.73	236.944	-52.6404	-3.43017
Z^4	6304.63	-659.764	162.85	-1.62112
Z^5	-15288.5	395.301	-83.6382	0
Z^6	18533.6	-67.5999	0	0
Z^7	-8719.48	0	0	0

Table A11. Same as in Table A10 but for the SDSS g band as a function of redshift and the $g-r$ colour.

	$(g-r)^0$	$(g-r)^1$	$(g-r)^2$	$(g-r)^3$
Z^0	0	0	0	0
Z^1	-0.962084	2.2796	4.16029	-3.27579
Z^2	15.6602	-14.8073	19.261	4.28022
Z^3	-82.9388	-49.2478	-40.9139	0
Z^4	273.308	131.339	0	0
Z^5	-312.677	0	0	0

Table A12. Same as in Table A10 but for the SDSS r band as a function of redshift and the $g-r$ colour.

	$(g-r)^0$	$(g-r)^1$	$(g-r)^2$	$(g-r)^3$
Z^0	0	0	0	0
Z^1	-0.351251	2.61848	-2.99032	1.59058
Z^2	1.93312	16.0682	-2.16736	-4.24709
Z^3	-69.9339	-49.337	22.9267	0
Z^4	253.373	12.0421	0	0
Z^5	-235.32	0	0	0

Table A13. Same as in Table A10 but for the SDSS i band as a function of redshift and the $g-i$ colour.

	$(g-i)^0$	$(g-i)^1$	$(g-i)^2$	$(g-i)^3$
Z^0	0	0	0	0
Z^1	-5.58619	8.51897	-3.44266	0.823935
Z^2	22.398	-31.8699	7.13812	-2.26748
Z^3	-16.5911	40.9251	6.77963	0
Z^4	-12.0117	-44.6466	0	0
Z^5	21.0947	0	0	0

Table A14. Same as in Table A10 but for the SDSS z band as a function of redshift and the $r-z$ colour.

	$(r-z)^0$	$(r-z)^1$	$(r-z)^2$	$(r-z)^3$
Z^0	0	0	0	0
Z^1	-1.426	3.08833	-0.726039	1.06364
Z^2	2.9386	-8.48028	-8.18852	-1.35281
Z^3	8.08986	53.5534	13.6829	0
Z^4	-93.2991	-77.1975	0	0
Z^5	133.298	0	0	0

Table A15. Same as in Table A10 but for the UKIDSS Y band as a function of redshift and the $Y-H$ colour.

	$(Y-H)^0$	$(Y-H)^1$	$(Y-H)^2$	$(Y-H)^3$
Z^0	0	0	0	0
Z^1	-2.62137	4.7578	2.28856	-4.02782
Z^2	29.4209	-26.5297	10.1083	10.5582
Z^3	-141.372	34.7785	-41.2725	0
Z^4	311.42	26.8742	0	0
Z^5	-264.997	0	0	0

APPENDIX B: K-CORRECTIONS CALCULATOR

To facilitate the usage of described analytical approximations and calculation of necessary K-corrections for user's data, we provide a dedicated web-site entitled "K-corrections calculator"[3] offering several ways of operation. Firstly, one can determine K-corrections for objects of interest one by one by manually filling interactive web form with the data available. This is the most straightforward method to determine K-corrections and it works in any modern web browser. As a second option, the ready-to-use code snippets written in popular data languages (C, IDL, Python) together with the corresponding analytical expressions are provided to simplify the integration of K-correction functionality into the user's code. Both ways allow a user to calculate K-corrections for SDSS *ugriz* and UKIRT WFCAM $YJHK$ (in AB magnitudes), but also for Johnson-Cousins $UBVR_cI_c$ and 2MASS JHK_s bands (in Vega magnitudes), choosing the most convenient colour as an input argument from several options. Based on user demands and feedback, we will consider the development of a web service for bulk calculation of K-corrections and publication of additional filter-colour combinations in the calculator.

[3] http://kcor.sai.msu.ru/

Table A16. Same as in Table A10 but for the UKIDSS J band as a function of redshift and the $J-K$ colour.

	$(J-K)^0$	$(J-K)^1$	$(J-K)^2$	$(J-K)^3$
Z^0	0	0	0	0
Z^1	-0.472236	2.1536	0.811858	-1.87211
Z^2	-0.107502	-8.00546	16.6955	4.85177
Z^3	-18.2002	-27.5709	-46.9334	0
Z^4	111.89	99.1294	0	0
Z^5	-162.057	0	0	0

Table A17. Same as in Table A10 but for the UKIDSS H band as a function of redshift and the $H-K$ colour.

	$(H-K)^0$	$(H-K)^1$	$(H-K)^2$	$(H-K)^3$
Z^0	0	0	0	0
Z^1	0.132484	1.93083	-4.7581	-6.67018
Z^2	8.61784	-17.3496	28.7714	8.05742
Z^3	-83.7003	267.725	127.193	109.678
Z^4	134.398	-1657.94	-851.199	-217.543
Z^5	567.048	4005.55	1071.17	0
Z^6	-2000.79	-3298.45	0	0
Z^7	1697.02	0	0	0

Table A18. Same as in Table A10 but for the UKIDSS K band as a function of redshift and the $J-K$ colour.

	$(J-K)^0$	$(J-K)^1$	$(J-K)^2$	$(J-K)^3$
Z^0	0	0	0	0
Z^1	-3.1771	1.66876	1.45967	-3.40684
Z^2	17.9897	-7.83528	13.3436	9.32974
Z^3	-114.067	-17.793	-42.0747	0
Z^4	318.424	70.0829	0	0
Z^5	-299.557	0	0	0

Table A19. Same as in Table A1 but for the Johnson U band as a function of redshift and the $U-R_c$ colour.

	$(U-R_c)^0$	$(U-R_c)^1$	$(U-R_c)^2$	$(U-R_c)^3$
Z^0	0	0	0	0
Z^1	2.84791	2.31564	-0.411492	-0.0362256
Z^2	-18.8238	13.2852	6.74212	-2.16222
Z^3	-307.885	-124.303	-9.92117	12.7453
Z^4	3040.57	428.811	-124.492	-14.3232
Z^5	-10677.7	-39.2842	197.445	0
Z^6	16022.4	-641.309	0	0
Z^7	-8586.18	0	0	0

Table A20. Same as in Table A1 but for the Johnson B band as a function of redshift and the $B-R_c$ colour.

	$(B-R_c)^0$	$(B-R_c)^1$	$(B-R_c)^2$	$(B-R_c)^3$
Z^0	0	0	0	0
Z^1	-1.99412	3.45377	0.818214	-0.630543
Z^2	15.9592	-3.99873	6.44175	0.828667
Z^3	-101.876	-44.4243	-12.6224	0
Z^4	299.29	86.789	0	0
Z^5	-304.526	0	0	0

Table A21. Same as in Table A1 but for the Johnson V band as a function of redshift and the $V-I_c$ colour.

	$(V-I_c)^0$	$(V-I_c)^1$	$(V-I_c)^2$	$(V-I_c)^3$
Z^0	0	0	0	0
Z^1	-1.37734	-1.3982	4.76093	-1.59598
Z^2	19.0533	-17.9194	8.32856	0.622176
Z^3	-86.9899	-13.6809	-9.25747	0
Z^4	305.09	39.4246	0	0
Z^5	-324.357	0	0	0

Table A22. Same as in Table A1 but for the Cousins R_c band as a function of redshift and the $B - R_c$ colour.

	$(B-R_c)^0$	$(B-R_c)^1$	$(B-R_c)^2$	$(B-R_c)^3$
Z^0	0	0	0	0
Z^1	-2.83216	4.64989	-2.86494	0.90422
Z^2	4.97464	5.34587	0.408024	-2.47204
Z^3	-57.3361	-30.3302	18.4741	0
Z^4	224.219	-19.3575	0	0
Z^5	-194.829	0	0	0

Table A23. Same as in Table A1 but for the Cousins I_c band as a function of redshift and the $V - I_c$ colour.

	$(V-I_c)^0$	$(V-I_c)^1$	$(V-I_c)^2$	$(V-I_c)^3$
Z^0	0	0	0	0
Z^1	-7.92467	17.6389	-15.2414	5.12562
Z^2	15.7555	-1.99263	10.663	-10.8329
Z^3	-88.0145	-42.9575	46.7401	0
Z^4	266.377	-67.5785	0	0
Z^5	-164.217	0	0	0